Contribution from the Departments of Physics and Chemistry,
University of Vermont, Burlington, Vermont 05405

Interaction of the Iron(III) Complex of *N*-[2-((*o*-Hydroxyphenyl)glycino)ethyl]salicylideneamine with Catechol and Cyanide: A Model for the Binding Site in the Dioxygenase Enzymes

K. Spartalian and Carl J. Carrano*

Received May 18, 1988

The interaction of *N*-[2-((*o*-hydroxyphenyl)glycino)ethyl]salicylideneamine, Fe(EHGS), with catechol and cyanide in aqueous solution has been investigated. Catechol appears to bind the iron center of Fe(EHGS) in a bidentate mode with a binding constant of log K = 10.6 (2) for the reaction Fe(EHGS) + $cat^{2-} \rightleftarrows$ Fe(EHGS)cat. The reaction of Fe(EHGS) with cyanide initially produces a violet high-spin monocyano complex via displacement of H_2O/OH in the sixth coordinating position. Further reaction yields a green low-spin tricyano species, which ultimately decays to ferricyanide. The kinetics of these reactions are consistent with this model. Analysis of the spectral properties of the cyano complexes of several phenolate-containing model compounds and non-heme iron proteins suggests that an anisotropic $g \approx 2.0$ EPR signal and a strong absorption band ($\epsilon_M \approx 900$-1500) in the 620-720-nm range may characterize *low-spin* Fe(III) tyrosinate proteins. It is proposed that the nitrile hydratases (*J. Am. Chem. Soc.* **1987**, *109*, 5848) may belong to this new group.

Introduction

Catechol 1,2-dioxygenase (CTD) and protocatechuate 3,4-dioxygenase (PCD) are bacterial non-heme iron enzymes which catalyze the oxidative cleavage of catechols to *cis,cis*-muconic acids.[1,2] They belong to a general class of proteins exhibiting iron-phenolate coordination[3] that also includes the purple acid phosphatases[4,5] and the transferrins.[6]

Recent resonance Raman studies have shown that the ferric ion at the active site of the dioxygenases is coordinated to one or more tyrosine ligands and that this coordination is not affected by substrate or oxygen binding.[7,8] Mössbauer spectroscopy reveals that the iron is maintained in the high-spin trivalent state throughout the catalytic cycle for all dioxygenases studied thus far.[2,9,10] This has led Que and co-workers to propose a unique mechanism whereby the iron activates the substrate for attack by molecular oxygen.[11] There has been considerable interest as to whether the substrate, catechol, binds in a monodentate or bidentate fashion to the iron. There is precedence for both forms,[12,13] and NMR evidence suggests that PCD and CTD may be different in this regard.[14]

Studies on the *Brevibacterium fuscum* protocatechuate 3,4-dioxygenase (which displays unusually sharp EPR and Mossbauer spectra) have clearly shown another interesting feature; the presence of one or more solvent water molecules in the coordination sphere of the iron in the resting enzyme.[15] It appears that this water remains coordinated upon binding many exclusively monodentate substrate analogues and inhibitors but is displaced by potentially bidentate substrates and cyanide.

The nature of the "water" site on these and other proteins has not been addressed. Specifically, given the high Lewis acidity of iron(III), is the water bound as H_2O or has it undergone hydrolysis to hydroxide? The true nature of the bound water is of considerable importance because this weakly occupied position is the apparent locus of interaction between the iron and external substances such as substrates or inhibitors. The coordinative unsaturation at the iron provided by the labile water is clearly an important feature with respect to its chemical reactivity.

In order to investigate this area, we have made use of quinquedentate model complexes containing donor groups similar to those implicated in the proteins and having an open coordination site where solvent water can bind.[16,17] Most useful in this regard has been the iron complex of *N*-[2-((*o*-hydroxyphenyl)glycino)-ethyl]salicylideneamine Fe(EHGS).[18,19] In aqueous solution, the coordinated water on Fe(EHGS) undergoes hydrolysis at nearly neutral pH, but uniquely the complex remains monomeric, yielding the simple hydroxo species rather than the μ-oxo dimer commonly seen. The Fe(EHGS) complex has already proved valuable in the study of the ionization state of the bound water in the iron binding site of the transferrins because of the distinctive signatures in the optical and Mossbauer spectra of its aquo and hydroxo forms.[18] In this report we extend the use of this model to the dioxygenases by examining its interaction with appropriate enzymatic substrates and inhibitors.

Experimental Section

Fe(EHGS) was prepared and purified as previously described.[18] Catechol was repeatedly resublimed before use. Solutions containing catechol were sparged with nitrogen and used immediately. All other chemicals were of the highest available commercial quality and were used as received.

Kinetic measurements were made at 25.5 °C by using a thermostated cell. Reactions were initiated by adding aliquots of a 2 M sodium cyanide solution, adjusted to the appropriate pH with HCl, to an approximately 3.0×10^{-4} M solution of Fe(EHGS). The reaction was followed spectrophotometrically at 500 nm.

Thermodynamic constants were measured by using methods previously described.[20] Data were fitted to the appropriate equations by using a

* Author to whom correspondence should be sent at Department of Chemistry, Southwest Texas University, San Marcos, TX 78666.

(1) Nozaki, M. *Top. Curr. Chem.* **1979**, *78*, 145-186.
(2) Whittaker, J. W.; Lipscomb, J. D.; Kent, T. A.; Munck, E. *J. Biol. Chem.* **1984**, *259*, 4466-4475.
(3) Que, L. *Coord. Chem. Rev.* **1983**, *50*, 73-108.
(4) Antanaitis, B. C.; Strakas, T.; Aisen, P. *J. Biol. Chem.* **1982**, *257*, 3766-3770.
(5) Davis, J. C.; Averill, B. A. *Proc. Natl. Acad. Sci. U.S.A.* **1982**, *79*, 4623-4627.
(6) Gaber, B. P.; Miskowski, V.; Spiro, T. G. *J. Am. Chem. Soc.* **1974**, *96*, 6868-6873.
(7) Keyes, W. E.; Loehr, T. M.; Taylor, M. L.; Loehr, J. S. *Biochem. Biophys. Res. Commun.* **1979**, *89*, 420-427.
(8) Que, L.; Heistand, R. H. *J. Am. Chem. Soc.* **1979**, *101*, 2219-2221.
(9) Que, L.; Lipscomb, J. D.; Munck, E.; Orme-Johnson, N. R.; Orme-Johnson, W. H. *Biochim. Biophys. Acta* **19768**, *452*, 320-334.
(10) Kent, T. A.; Munck, E.; Pyrz, J. W.; Widom, J.; Que, L. *Inorg. Chem.* **1987**, *26*, 1402-1408.
(11) Que, L.; Lipscomb, J. D.; Munck, E.; Wood, J. M. *Biochem. Biophys. Acta* **1977**, *485*, 60-64.
(12) Heistand, R. H.; Roe, A. L.; Que, L. *Inorg. Chem.* **1982**, *21*, 676-681.
(13) White, L. S.; Nilsson, P. V.; Pignolet, L. H.; Que, L. *J. Am. Chem. Soc.* **1984**, *106*, 8312-8313.
(14) Lauffer, R. B.; Que, L. *J. Am. Chem. Soc.* **1982**, *104*, 7324-7325.
(15) Whittaker, J. W.; Lipscomb, J. D. *J. Biol. Chem.* **1984**, *259*, 4487-4495.
(16) Spartalian, K.; Carrano, C. J. *J. Chem. Phys.* **1983**, *78*, 4811-4816.
(17) Patch, M. G.; Simolo, K. P.; Carrano, C. J. *Inorg. Chem.* **1983**, *22*, 2630-2634.
(18) Carrano, C. J.; Spartalian, K.; Appa Rao, G. V. N.; Pecoraro, V. L.; Sundaralingam, M. J. *J. Am. Chem. Soc.* **1985**, *107*, 1651-1658.
(19) Spartalian, K.; Carrano, C. J. *Inorg. Chem.* **1984**, *23*, 1993-1995.
(20) Harris, W. R.; Carrano, C. J.; Raymond, K. N. *J. Am. Chem. Soc.* **1979**, *101*, 2722-2727.

0020-1669/89/1328-0019$01.50/0

Table I. Formation Constants of Selected Phenolate-Containing Chelates

ligand[a]	log K_{ML}	log K_{OH}	ref
HBED	39.7		23
rac-EHPG	35.0	12.6	24
meso-EHPG	33.8	10.3	24
EHGS	33.3	6.7	this work
SALEN	25.8		25

[a] See Chart I for structures.

Chart I

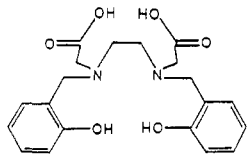

N,N'-bis(*o*-hydroxybenzyl)ethylenediamine-*N,N'*-diacetic acid

HBED

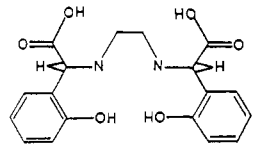

N,N'-ethylenebis((*o*-hydroxyphenyl)glycine)

EHPG

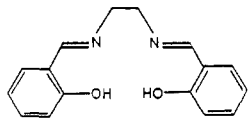

N,N'-disalicylideneethylenediamine

SALEN

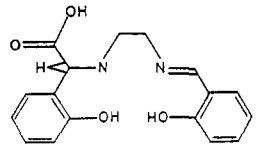

N-[2-(salicylideneamino)ethyl]-(*o*-hydroxyphenyl)glycine

EHGS

least-squares fitting simplex algorithm.

NMR spectra were obtained in the appropriate deuteriated solvents on a Bruker 270-MHz spectrometer and are referenced to internal TMS. EPR and Mössbauer spectroscopies were performed as previously described.[18] All optical measurements employed a Perkin-Elmer 553 fast-scan spectrophotometer.

Results and Discussion

Formation Constant for Fe(EHGS). If we view complexes such as Fe(EHGS) as reasonable structural models for the dioxygenase enzymes, then the formation constant of Fe(EHGS) may give some indication of the potential stability of the analogous metalloproteins. Because free EHGS is unstable in solution and its formation constant with iron is expected to be very high, direct measurements by potentiometric titration were deemed unsuitable. Instead, the stability constant was determined spectrophotometrically by competition with EDTA as described by eq 1. Using

$$Fe(EHGS) + EDTA^{4-} + 3H^+ \rightarrow Fe(EDTA)^- + H_3EHGS \quad (1)$$

the known value for the formation constant of the ferric–EDTA complex[21] and measuring [Fe(EHGS)] by the loss in intensity of the LMCT band at 497 nm, it is possible to calculate the standard formation constant from the appropriate mass balance equations. The formation constant K_{ML} can then be expressed as

$$K_{ML} = \frac{[Fe(EHGS)]}{[Fe^{3+}][EHGS^{3-}]} \quad (2)$$

This expression requires knowledge of the ligand protonation constants, which although they cannot be determined direclty, can be estimated from the data provided by Martell et al. for the similar ligand, EHPG.[22] Using these values results in a measured

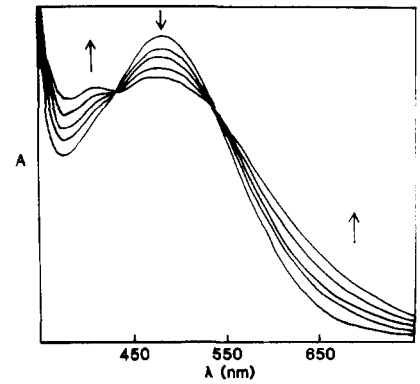

Figure 1. Optical changes accompanying the addition of catechol to an 1.8×10^{-4} M solution of Fe(EHGS) in 50 mM HEPES buffer, pH 7.6. The first scan represents addition of 0 equiv of catechol; successive spectra correspond to additions of 1.4, 2.8, 5.6, and 9.8 equiv, respectively. Arrows indicate the direction of change in the absorption bands.

formation constant log K_{ML} = 33.3 (2) at 25 °C in 0.1 M KNO_3. Table I shows the formation constants of the similar hexadentate chelates Fe(EHPG) and Fe(HBED) for comparison. Structures of the complexes discussed in Table I can be found in Chart I.

The increased stability of HBED over EHPG has been attributed to a more favorable steric arrangement of the carboxyl groups. The increase in stability of the *rac* isomer of EHPG over the meso isomer is a reflection of the unfavorability of placing the six-membered phenolate chelate ring in an apical position as required by the meso geometry. The loss in stability for EHGS, which like *rac*-EHPG has both phenols equatorial, is presumably a measure of the binding strength contributed by a carboxyl group. The effect is clearly small, and we can infer that most of the high overall stability in these molecules is attributable to the highly basic phenolates.

The values of the hydrolysis constants for the various chelates are also listed in Table I. There is frequently a direct correlation between the magnitude of the formation constant log K_{ML} with the corresponding chelate hydrolysis constant (see ref 20). While the trend of decreasing hydrolysis constant with decreasing overall stability is seen, the magnitude of the EHGS hydrolysis constant is about 3 orders of magnitude less than expected. This is presumably a result of the open coordination site in the pentacoordinate Fe(EHGS), which renders hydrolysis more facile than for the corresponding coordinatively saturated hexadentate complexes where a ligand arm must be displaced. Thus hydrolysis can be expected to be facile in the dioxygenase enzymes, which also have open coordination sites.

Reactions with Catechol and Other Phenols. When enzyme substrates or pseudosubstrates such as benzoate or a variety of phenols are added to an aqueous solution of Fe(EHGS) at pH 7.6, spectral changes indicative of binding are seen. However the small changes and the required high concentrations make systematic studies difficult. Apparently, monodentate phenols in aqueous solution bind so weakly to the iron center of Fe(EHGS) that they cannot compete with the solvent as an axial ligand. In organic solvents, phenols have been seen to bind much more tightly to the iron in the related model system Fe(SALEN).[26,27] Presumably hydrophobic and/or other secondary interactions are also important for stabilizing these weakly bound ligands in the dioxygenase enzymes themselves.

While monodentate phenols etc. bind only weakly to the iron center in Fe(EHGS), potentially bidentate substrates like catechol are found to have a high affinity. When aliquots of catechol are added to a solution of Fe(EHGS) at pH 7.6, characteristic spectral

(21) Martell, A. E.; Smith, R. M. *Critical Stability Constants*; v. 1, Plenum Press: New York, 1975; Vol. 1, pp 294–311.
(22) Frost, A. E.; Freedman, H. H.; Westerback, S. J.; Martell, A. E. *J. Am. Chem. Soc.* **1958**, *80*, 530–535.
(23) Eplattenier, F. L.; Murase, I.; Martell, A. E. *J. Am. Chem. Soc.* **1967**, *89*, 837–843.
(24) Bernauer, K. *Top. Curr. Chem.* **1976**, *65*, 1.
(25) Lloret, F.; Moratal, J.; Faus, J. *J. Chem. Soc., Dalton Trans.* **1983**, 1749–1753.
(26) Heistand, R. H.; Lauffer, R. B.; Fikrig, E.; Que, L. *J. Am. Chem. Soc.* **1982**, *104*, 2789–2796.
(27) Pyrz, J. W.; Roe, A. L.; Stern, L. J.; Que, L. *J. Am. Chem. Soc.* **1985**, *107*, 614–620.

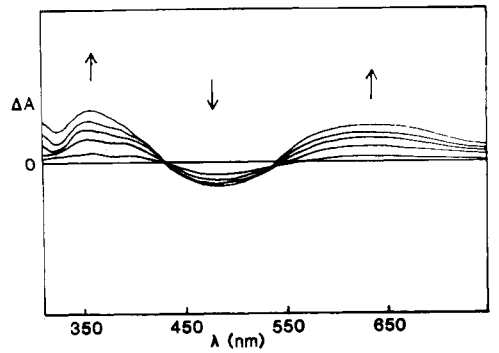

Figure 2. Difference spectrum for the addition of catechol to an 2.0×10^{-4} M solution of Fe(EHGS) in 50 mM HEPES buffer, pH 7.3.

changes such as those shown in Figure 1 are seen. As increasing amounts of catechol are added, the peak at about 470 nm begins to decrease, with the formation of a new peak that is blue-shifted to 400 nm and an increase in the absorbance in the red. Two isosbestic points are observed at 430 and 530 nm. The nature of the new peaks is more readily seen in a difference spectrum, Figure 2, which clearly shows the formation of new bands at 360, 400, and 625 nm as increasing amounts of catechol are added. After about 10 equiv of catechol have been added, the initial absorbance changes begin to diminish and the isosbestic points are lost. At very high catechol concentrations, formation of $Fe(cat)_3^{3-}$ is observed as the catechol begins to displace the entire EHGS ligand.

We propose that the following reaction is occurring:

$$Fe(EHGS) + H_2cat \rightleftarrows Fe(EHGS)cat + nH^+ \quad (3)$$

Thus the pH-dependent equilibrium expression is[28]

$$K^* = \frac{[Fe(EHGS)cat][H^+]^n}{[Fe(EHGS)][H_2cat]} \quad (4)$$

where n can be 1 or 2 depending on whether catechol binds in a monodentate or bidentate fashion. The constant K^* can be determined spectrophotometrically by using the usual mass balance and equilibrium equations and was refined by nonlinear least-squares refinement of

$$A(x) = \frac{A_0 - A_\infty}{1 + K^*[H_2cat]} \quad (5)$$

where $A(x)$ is the absorbance at some concentration of added catechol, A_0 is the initial absorbance (no catechol added), and A_∞ is the absorbance when the Fe(EHGS)cat complex is fully formed. Parameters K^* and A_∞ were varied to get the best fit.[29] The normal pH-independent metal–ligand formation constant can be calculated from K^* by

$$K_{ML} = K^*/\beta_2 \quad (6)$$

where β_2 is the sum of the catechol K_a's.[30] Fits at several pH values using a value of β_2 of 6.03×10^{-23} give log $K_{ML} = 10.6$ (2).

In solving the equilibrium expression (eq 4), we have assumed two-proton stoichiometry, which implies bidentate catechol coordination. Considering that there is precedence for monodentate catechol binding, it was necessary to ascertain whether our choice of proton stoichiometry was correct by examining the pH dependence of the formation of Fe(EHGS)cat. When the pH of a solution of Fe(EHGS) containing a 10-fold excess of catechol is varied from 6.1 to 7.9, characteristic spectral changes are once again observed, indicative of increasing formation of Fe(EHGS)cat. The presence of apparent pseudoisosbestic points is surprising since there are clearly at least three species whose concentrations are changing over this range; $Fe(EHGS)H_2O$, Fe(EHGS)OH, and Fe(EHGS)cat.[31] The data were again analyzed by nonlinear least-squares refinement, and significantly better fits were obtained for n = 2 than for $n = 1$. The χ^2 for $n = 2$ was smaller than that for $n = 1$ by a factor of 8. The calculated log K_{ML} of 10.2 agrees reasonably well with the value obtained from the concentration dependence.

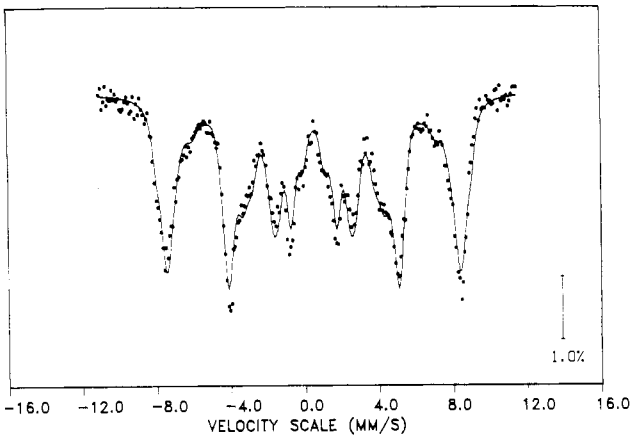

Figure 3. Mössbauer spectrum of Fe(EHGS)cat in frozen 5:1 glycerine/H_2O solution at 4.2 K in a 130-mT applied field transverse to the γ-beam. The solid line shows the fit to a spin Hamiltonian as described in the text.

Table II. Mössbauer Parameters for Fe(EHGS)cat

$D = 0.75\ cm^{-1}$; $\lambda = 0.24$
$A/g_n\beta_n = -21.6$ T (excited state)
$\delta = 0.5$ mm/s; $\Delta E = 0.0$

The spectral changes seen when catechol reacts with Fe(EHGS) are consistent with coordination of the catechol at the iron center. The shifting of the EHGS phenolate-to-iron CT band to higher energy and the appearance of the catechol-to-iron CT at 626 nm are in accord with the expectations based on the work of Que and co-workers with the nonaqueous-based Fe(SALEN)X series.[26,27] In particular, it is consistent only with a chelated mode of catechol binding rather than a protonated or deprotonated monodentate mode. The two-proton stoichiometry found upon catechol binding and the magnitude of the formation constant are also consistent only with a bidentate catechol. The average value of log K_{ML} of 10.4 (2) is much higher than that expected for a monodentate phenol type interaction (log $K_{ML} \approx 2$) but is considerably less than that found for bidentate catechol binding to Fe(SALEN)X.[25] We suggest that this weaker binding of catechol to Fe(EHGS) as compared with that to Fe(SALEN) may reflect the need for catechol to displace a ligand arm (presumably the carboxylate) in order to coordinate in a bidentate mode. Such is not necessary with the tetradentate SALEN although an unfavorable twisting of the normally planar ligand is required to achieve cis coordination of the catechol. The weaker binding of catechol to Fe(EHGS) as compared with that to Fe(SALEN) is reflected in the difference in energy between the ligand phenolate-to-Fe and the catecholate-to-Fe CT bands. This difference is smaller in EHGS than in SALEN. Thus the Fe(EHGS)cat complex appears blue-brown and does not show a distinct catechol-to-Fe CT band while Fe(SALEN)cat is bright green and has a well-resolved band. Upon anaerobic addition of catechol the dioxygenase enzymes themselves change from red to a blue-gray or blue-brown color and do not show a distinct catechol-to Fe CT band, suggesting relatively weak bidentate catechol binding in the ES complex.

(28) The equilibrium as written here is based on the aquo form of Fe(EHGS), but an equivalent expression can be written for the hydroxo form.
(29) It was necessary to refine A_∞ because at catechol concentrations sufficient to drive the reaction to completion, formation of $Fe(cat)_3^{3-}$ became a significant interference.
(30) Avdeef, A. E.; Sofen, S. R.; Bregante, T. L.; Raymond, K. N. *J. Am. Chem. Soc.* **1978**, *100*, 5362–5370.
(31) Whether the catechol reacts with the Fe(EHGS)OH or $Fe(EHGS)H_2O$ form preferentially cannot be determined from equilibrium measurements but is under active kinetic investigation.

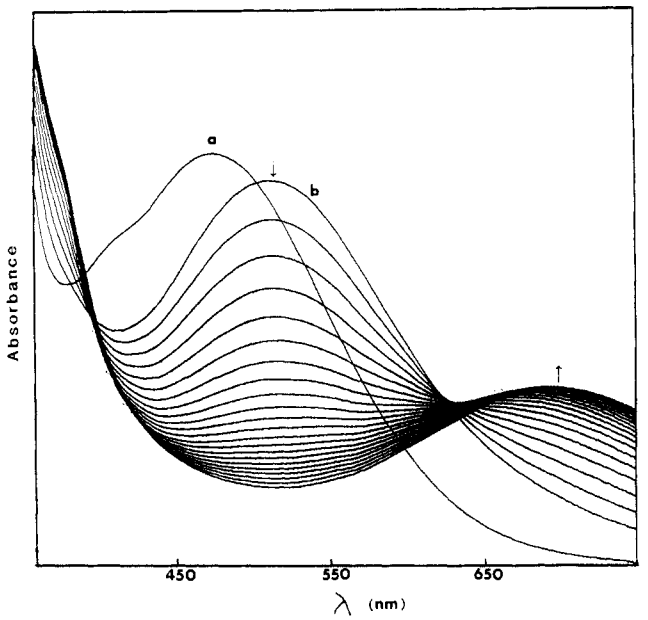

Figure 4. Time-dependent spectral changes accompanying cyanide addition (total concentration 0.6 M) to a 3.0×10^{-4} M solution of Fe(EHGS), pH 8.0. Successive scans are 10 min apart. Spectrum a was obtained from Fe(EHGS) in the absence of cyanide; spectrum b was obtained immediately after cyanide addition.

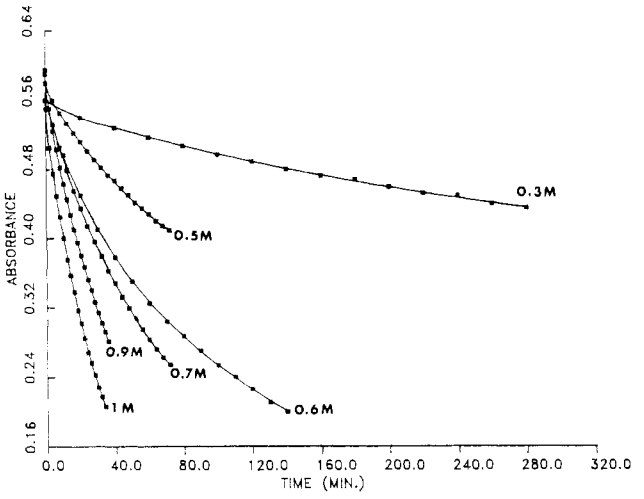

Figure 5. Absorbance at 500 nm vs time for the additions of various concentrations of cyanide to 3.0×10^{-4} M Fe(EHGS), pH 8.0. The points represent measured data, and the solid lines are fits based on the model described in the text.

We have also analyzed the binding of catechol to Fe(EHGS) by Mössbauer spectroscopy. Figure 3 shows the Mössbauer spectrum of a frozen solution at 4.2 K in an external magnetic field of 130 mT applied transversely to the direction of the γ-beam. The spectrum was analyzed in terms of the standard spin Hamiltonian

$$\mathcal{H} = D[S_z^2 - S(S+1)/3 + \lambda(S_x^2 - S_y^2)] + 2g\beta\vec{H}\cdot\vec{S} \quad (7)$$

with $S = 5/2$ following the least-squares-fitting procedure described in ref 16. The solid line represents a calculation based on the best parameters shown in Table II. These parameters are typical of high-spin Fe(III) "$g = 4.3$" complexes. A noteworthy feature of the spectrum is its left-to-right symmetry interpreted as the absence of quadrupole interaction. This indicates a nearly spherical charge distribution about the nucleus.

Reaction with Cyanide. When an excess of cyanide is added to a solution of Fe(EHGS) at nearly neutral pH, the rapid formation of a new species is observed as indicated by a change in color from red to violet. This violet intermediate decays over a period varying from minutes to hours to a pale green complex.

Table III. Kinetic Parameters for Sequential Cyanide Addition to Fe(EHGS)

cyanide concn, M	rate consts, min^{-1}		
	k_1	k_2	k_3
0.3	1.0	3.6×10^{-3}	1.0×10^{-4}
0.5	1.4	1.55×10^{-2}	1.8×10^{-3}
0.6	0.8	3.26×10^{-2}	5.5×10^{-3}
0.7	1.0	3.86×10^{-2}	8.8×10^{-3}
0.9	0.9	5.82×10^{-2}	1.77×10^{-2}
1.0	0.9	9.43×10^{-2}	2.72×10^{-2}

Average Extinction Coefficients (± Standard Deviation)

ϵ_1 = 1910 (60) L/(mol cm) ϵ_3 = 1180 (30) L/(mol cm)

ϵ_2 = 1830 (57) L/(mol cm) ϵ_4 = 10 (1) L/(mol cm)

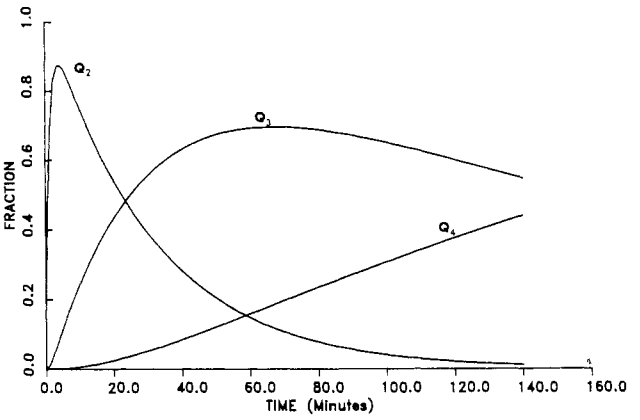

Figure 6. Time course for the formation and decay of species Q_2, Q_3, and Q_4 (see text) for 0.6 M cyanide, 3.0×10^{-4} M Fe(EHGS), and pH 8.0.

Over even longer periods the solution becomes bleached. Typical spectral changes are shown in Figure 4. The initial reaction results in a red shift of the LMCT band from 470 to 510 nm with little change in extinction coefficient. Further reaction results in a slow additional red shift to 700 nm with a loss in intensity.

Figure 5 shows the absorbance, at $\lambda = 500$ nm, as function of time for six different concentrations of cyanide. The data were fitted to theoretical models by the method of least squares using a simplex algorithm. The simplest model that can fit all the data has the starting material Fe(EHGS) (Q_1) decaying to the final product (Q_4) through two intermediates (Q_2 and Q_3). We identify Q_2 as the purple intermediate and Q_3 as the green intermediate. This model requires seven parameters: four extinction coefficients and three pseudo-first-order rate constants. Simpler models yielded poorer fits as evidenced by significantly higher values of χ^2 and by unphysical results such as negative rate constants or extinction coefficients that varied systematically with cyanide concentration. We believe that the two-intermediate model is an appropriate description because it fits the data well, is self-consistent and is chemically reasonable. Table III summarizes the pseudo-first-order rate constants and average extinction coefficients obtained from the fits.

The equations that govern the time development of the starting material and the intermediates are proportional to the total concentration $[Q_0]$ and are given by

$$[Q_1] = [Q_0]\exp(-k_1 t) \quad (8a)$$

$$[Q_2] = \frac{k_1[Q_0]}{k_2 - k_1}[\exp(-k_1 t) - \exp(-k_2 t)] \quad (8b)$$

$$[Q_3] = k_1 k_2 [Q_0]\left[\frac{\exp(-k_1 t)}{(k_2 - k_1)(k_3 - k_1)} - \frac{\exp(-k_2 t)}{(k_2 - k_1)(k_3 - k_2)} + \frac{\exp(-k_3 t)}{(k_3 - k_1)(k_3 - k_2)}\right] \quad (8c)$$

$$[Q_4] = [q_0] - ([Q_1] + [Q_2] + [Q_3]) \quad (8d)$$

When k_1 is greater than k_2 and k_3 by an order of magnitude (or more) as is the case here, the starting material decays too

Scheme I

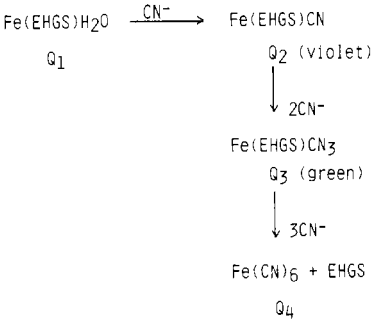

rapidly to permit a reliable determination of k_1 with our available instrumentation. For this reason we attach little significance to the entires for this rate constant in Table III. Figure 6 shows the time course for the formation and disappearance of the various species involved at a cyanide concentration of 0.6 M. As can be seen, the first intermediate (violet) decays quickly, while the second (green) intermediate is virtually in a steady state.

We were unable to record satisfactory Mössbauer or EPR spectra on the violet intermediate. However EPR spectroscopy performed on the green intermediate showed a clean rhombic signal centered at 2 (g = 2.37, 2.18, 1.93) indicative of *low-spin ferric ion*. The Mossbauer spectrum corroborated this interpretation and showed an additional EPR silent component that we attribute to ferrocyanide.

A mechanism for the addition of cyanide to Fe(EHGS) that is consistent with the kinetic evidence, as well as the optical and magnetic resonance spectroscopy, can be envisioned. We propose that the initial violet intermediate forms from the rapid displacement of the H_2O on Fe(EHGS)(H_2O) by CN^- ion. Plots of the pseudo-first order rate constant vs $(CN^-)^2$ for the conversion of the violet intermediate (Q_2) into the green species (Q_3) are linear and suggest a second-order process. The second-order rate constant is 2.67×10^{-2} M^{-1} min^{-1}. This reaction apparently involves the addition of two cyanide ions to Fe(EHGS)CN to form a *low-spin* Fe(EHGS)$(CN)_3$ complex as determined by EPR spectroscopy. The pH dependence of this reaction also exhibits an inverse second-order hydrogen ion dependence, consistent with the second-order cyanide dependence and indicating that CN^- is the reactive species rather than HCN.

Clearly several of the ligand donors from the EHGS must be displaced from Fe(EHGS)CN to form Fe(EHGS)CN_3. While we expected that the carboxylate oxygen trans to the cyanide would be labilized and easily displaced, the identity of the other donor atom displaced is unclear. Either a phenolate oxygen or the amine or imine nitrogen could be involved. Analysis of the optical spectrum of the green intermediate suggests that the phenols are still bound (vide infra); thus we favor either the amine or imine nitrogen as the displaced atom.

Analysis of the third reaction $Q_3 \rightarrow Q_4$ suggests that it involves an additional three cyanides (plots of k_{obs} vs cyanide concentration are linear only for $[CN]^3$) to displace completely the EHGS ligand and produce a hexacyanide (see Scheme I).

The reaction of cyanide with the *B. fuscum* protocatechuate 3,4-dioxygenase is remarkably similar.[15] Rapid addition of one cyanide ion, presumably by displacement of the coordinated $H_2O/(OH)$ occurs first, leading to a high-spin, violet, monocyano complex ($\lambda_{max} \approx 540$ nm). This in turn undergoes a slow addition of more cyanide to yield a green low-spin complex. The exact molecularity of this second step remains undetermined. A low-spin tricyano species with g values similar to the ones reported here for Fe(EHGS) is also observed in the interaction of the iron-tyrosinate protein transferrin with excess cyanide.[32]

Oxidative Cleavage of *tert*-Butylcatechol by Fe(EHGS). Despite its ability to bind catechol tightly and its many physiochemical similarities to the native dioxygenases enzymes, Fe(EHGS) is not a particularly efficient catalyst. When Fe(EHGS) and *tert*-butyl catechol were mixed in pH 8.3 borate/DMF buffer, the initially brown solution gradually turned green. The products were extracted after the mixture was stirred in air for 4 days, separated by preparative TLC and analyzed by NMR spectroscopy. The major product was *tert*-butylquinone although significant amounts of several lactones expected from the ring cleavage products were also produced. Despite the production of ring cleavage products by Fe(EHGS), the system is unremarkable; many others have been described that are far more efficient and produce no quinone.[33-36]

(32) Chasteen, N. D. Personal communication.

Table IV. Comparison of Physical Parameters for *B. fuscum* Protocatechuate 3,4-Dioxygenase, Fe(EHGS)OH, and Fe(EHGS)H_2O

param	*B. fuscum*	Fe(EHGS)OH	Fe(EHGS)H_2O
λ_{max}, nm	435	440	497
ϵ_M (per iron)	2900	2900	4000
Γ, mm/s	0.33	0.39	0.53
A_0, MHz	29.1	30.5	28.6
D, cm^{-1}	1.4	1.7	0.16
λ	0.33	0.34	0.97[a]
ϵE, mm/s	0.40	0.42	1.60
δ, mm/s	0.44	0.50	0.54
H_{sat}, T	−53	−55	−51.5

[a] This complex also has a quartic parameter μ = −1.45.

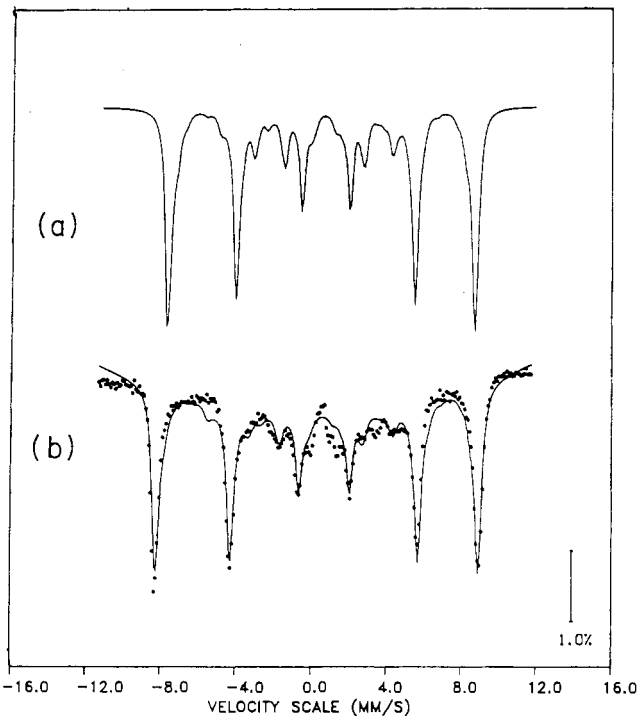

Figure 7. (a) Mössbauer spectrum for *B. fuscum* at 4.2 K in a 130-mT transverse field calculated from the parameters reported in ref 10. (b) Mössbauer spectrum of Fe(EHGS)OH under the same conditions modified from ref 18.

Discussion

We have now accumulated a substantial amount of data based on our model complex Fe(EHGS) that suggests that the ionization state of the water bound to iron can be discerned. Clear differences in the optical, EPR, and Mössbauer spectra are all evident between water and hydroxide binding. We have used this information previously to suggest that both the aquo and the hydroxy forms of the bound water may coexist in the iron transport protein ovotransferrin. Comparison of the data for Fe(EHGS)OH, Fe-

(33) Funabiki, T.; Mizoguchi, A.; Sugimoto, T.; Tada, S.; Tsuji, M.; Sakamoto, H.; Yoshida, S. *J. Am. Chem. Soc.* **1986**, *108*, 2921–2932.
(34) Weller, M. G.; Weser, U. *J. Am. Chem. Soc.* **1982**, *104*, 3752–3754.
(35) Weller, M. G.; Weser, U. *Inorg. Chim. Acta* **1985**, *107*, 243–245.
(36) Que, L.; Kolanczyk, R. C.; White, L. S. *J. Am. Chem. Soc.* **1987**, *109*, 5373–5380.

(EHGS)H_2O, and *B. fuscum* protocatechuate 3,4-dioxygenase (Table IV) suggests that the enzyme contains coordinated hydroxide. This is revealed perhaps more clearly by comparison of a simulation of the Mössbauer spectra from *B. fuscum* with that from Fe(EHGS), Figure 7. The only significant difference in parameters between the two is in the magnetic hyperfine coupling constant A. The reduced value of A in *B. fuscum* is an indication of increased covalency in the metal–ligand bonds. This is not unexpected since the imino/amino nitrogens in the model are expected to form less covalent bonds with the iron than the aromatic imidazole nitrogens thought to be present in the enzyme.[2,37] In the related enzyme, catechol 1,2-dioxygenase from *Pseudomonas putida*, several species of iron are clearly present in the Mössbauer spectra described by Munck et al.[10] We attribute that feature described by them as *B. fuscum*-like as arising from coordinated hydroxide by analogy to the above. While we cannot determine the nature of the other minor components, they are clearly not aquo-like.

We were intrigued by the nature of the changes in the optical spectrum of Fe(EHGS) in the presence of cyanide. The red shift upon addition of the first cyanide is clearly not a charge effect, as an increasing negative charge would be expected to shift the phenolate oxygen-to-iron CT band to higher energy.[37] This is seen for example when water is ionized to hydroxide, i.e. Fe(EHGS)H_2O for which λ_{max} = 490 nm and Fe(EHGS)OH for which λ_{max} = 440 nm. The shift to lower energy of the LMCT must be the result of a lowering of the iron t_{2g} electron manifold by the strong-field cyanide ion.

The situation is less clear after the addition of further cyanide ions. Here the original band is bleached with the appearance of a new unassigned feature at 700 nm. This is accompanied by a change in spin state from high spin to low spin as indicated by the EPR measurements. While the nature of the original band as a phenolate-to-metal CT band is clear, the origin of the 700-nm feature is obscure. In particular we wished to known if the phenolates remain coordinated after cyanide binding. Two observations convince us that the 700-nm band is in fact a characteristic feature of phenolate-to-iron charge-transfer transitions involving low-spin Fe(III).

The most direct evidence comes from a series of hexadentate phenolate-containing ligands reported by Wilson and co-workers.[38,39] These iron complexes are near the high-spin to low-spin cros ,over point. They all possess the characteristic red to violet colors and ~490 nm absorption bands in their high-spin configurations, indicative of phenolate-to-metal CT transitions. However by lowering the temperature, it is possible to initiate a spin change to the $S = {}^1/_2$ state *without introducing any new ligands*. This results in a color change from red to green and the loss of the 490 nm ($\epsilon_M \approx 3600$) CT band and the growth of a new band at 620 nm ($\epsilon_M \approx 1900$) indicative of the low-spin state.

A theoretical basis for these observations can be obtained from Jørgenson's optical electronegativity theory.[40,41] Details can be found in the cited references, but a brief account is in order. Equation 9 has been found to correlate the transition energies of LMCT bands for a wide range of metal ions and ligands

$$\nu_{cor} = 30(X_L - X_M) \quad (9)$$

where X_L and X_M are the optical electronegativities of the ligand and the metal respectively. The values appropriate for iron(III) and phenolate ligands are known.[42] The value of ν_{cor} is the transition energy of the first allowed CT band corrected for interelectronic repulsion and ligand field effects. The interelectronic repulsion effects are determined from differences in the spin-pairing energy Δ(SPE) between the initial and final states where

$$\mathrm{SPE} = \left[\frac{3}{4}n\left(1 - \frac{n-1}{9}\right) - S(S+1)\right]D \quad (10)$$

In this equation n = number of d electrons, $D \approx 7B$, where B is the effective Racah parameter, and S has its usual meaning. This approach allows one to predict the position of a phenolate-to-metal CT band for iron(III) in a low-spin configuration since when the spin state changes, the spin-pairing energy changes, in turn leading to the change in the position of the CT band. A simple calculation leads to a predicted value of 684 nm for the phenolate-to-metal charge-transfer band in the low-spin system, assuming a band at 470 nm for the high-spin form. This analysis neglects the fact that the softer cyanide ion in addition to changing the spin state also increases the covalency, i.e. reduces B (the so called nepheloauxetic effect). Reducing the Racah parameter by 5% from that used in the EHPG models to account for the CN^- covalency, leads to a predicted value of 700 nm, which matches that observed in the low-spin green intermediate. The low-spin form of the cyanide-treated *B. fuscum* enzyme displays a similar band at 620 nm, and low-spin Fe(SALEN)$(CN)_2$ displays a band at 715 nm.[43] Both species are green.

In the same way that a g = 4.3 EPR signal and an intense optical band in the 450–500-nm region have served to characterize high-spin non-heme iron proteins with iron–tyrosinate coordination,[6] we suggest that an anisotropic $g \approx 2.0$ EPR signal and strong absorption band ($\epsilon_M \sim$ 900–1500) in the 620–720-nm range characterize low-spin Fe(III) tyrosinate proteins. Indeed a series of iron-containing enzymes fitting this description have recently been reported.[44-46] The nitrile hydratases, bacterial enzymes catalyzing the hydration of aliphatic nitriles to the corresponding amides, are reported to have EPR signals at 2.28, 2.14, and 1.97 and an absorption band at about 710 nm (ϵ_M = 700–1100/iron). Little is known about the coordination environment other than the iron itself is low-spin Fe(III) with the probable presence of a water molecule as a ligand. We suggest that these green-colored enzymes contain one or more tyrosines as ligands and that the phenolate- to low-spin Fe(III) CT is responsible for the absorption band at 700 nm. Resonance Raman spectroscopy should be able to prove the point definitively.

Acknowledgment. This work was supported by a grant from the NSF Vermont EPSCoR.

Registry No. Fe(EHGS) complex, 94706-21-5; CN^-, 57-12-5; catechol, 120-80-9.

(37) Ainscough, E. W.; Brodie, A. M.; Plowman, J. E.; Brown, K. L.; Addison, A. W.; Gainsford, A. R. *Inorg. Chem.* **1980**, *19*, 3655–3663.
(38) Tweedle, M. F.; Wilson, L. J. *J. Am. Chem. Soc.* **1976**, *98*, 4824–4834.
(39) Sinn, E.; Sim, G.; Dose, E. V.; Tweddle, M. F.; Wilson, L. J. *J. Am. Chem. Soc.* **1978**, *100*, 3375–3390.
(40) Jørgenson, C. K. *Acta Chem. Scand.* **1962**, *16*, 2406–2410.
(41) Jørgenson, C. K. *Mol. Phys.* **1963**, *6*, 44–47.
(42) Patch, M. G.; Carrano, C. J. *Inorg. Chim. Acta* **1981**, *56*, L71–L73.
(43) Nishida, Y.; Oshio, S.; Kida, S. *Bull. Chem. Soc. Jpn.* **1977**, *50*, 119–122.
(44) Sugiura, Y.; Kuwahara, J.; Nagasawa, T.; Yamada, H. **1987**, *J. Am. Chem. Soc. 109*, 5848–5850.
(45) Nagasawa, T.; Ryuno, K.; Yamada, H. *Biochem. Biophys. Res. Commun.* **1986**, *139*, 1305–1312.
(46) Nagasawa, T.; Nanba, H.; Ryono, K.; Takeuchi, K.; Yamada, H. *Eur. J. Biochem.* **1987**, *162*, 691–698.